Defect and Diffusion Forum
ISSN: 1662-9507, Vol. 450, pp 31-39
doi:10.4028/p-9AOMkv

Submitted: 2025-12-22
Revised: 2026-02-16
Accepted: 2026-02-22
Online: 2026-04-15

Cryogenic Machining of a Laser Powder Bed Fusion-Processed AlSi7Mg Aluminum Alloy

Rachele Bertolini[1,a*], Toushiqul Islam[2,b], Shuaihang Pan[2,c], Edoardo Ghinatti[1,d] and Stefania Bruschi[1,e]

[1]Department of Industrial Engineering, University of Padova, Via Venezia, 1, 35131, Padova, Italy

[2]Lab of Advanced Manufacturing (LoAM), Department of Mechanical Engineering, University of Utah, Salt Lake City, UT, 84112, USA

[a]rachele.bertolini@unipd.it, [b]toushiqul.islam@utah.edu, [c]Shuaihang.Pan@utah.edu, [d]edoardo.ghinatti@phd.unipd.it, [e]stefania.bruschi@unipd.it

Keywords: Laser powder bed fusion, aluminum alloy, machinability, surface integrity, EBSD, layer thickness.

Abstract. Additive manufacturing by laser powder bed fusion (LPBF) is increasingly applied to aluminium alloys; however, the resulting surface quality and machining behaviour remain critical challenges, particularly when post-processing is required. In this context, the interaction between LPBF process parameters and advanced cooling strategies during machining remains largely unexplored.

This study examines the impact of cryogenic machining on the surface integrity of LPBF-produced AlSi7Mg components, fabricated with varying layer thicknesses. Specimens were machined under fixed cutting parameters using either conventional flood cooling or cryogenic cooling. Cutting forces, surface roughness, defect morphology, and subsurface microstructure were systematically evaluated. Cryogenic cooling consistently reduced cutting forces and improved surface quality, effectively suppressing tearing formation. In contrast, under flood cooling, the influence of the microstructural differences induced by layer thickness remained significant, with increasing LPBF layer thickness further enhancing both surface and subsurface integrity. Overall, the results reveal a strong interaction between LPBF parameters and cooling strategy, highlighting the unexpectedly beneficial role of cryogenic machining in improving the surface integrity of LPBF-processed AlSi7Mg alloys.

Introduction

Aluminum alloys offer attractive properties such as an excellent strength-to-weight ratio and good corrosion resistance. In recent years, additive manufacturing, particularly laser powder bed fusion (LPBF), has been increasingly adopted for the production of lightweight and geometrically complex aluminum alloy components due to its high design flexibility. Variations in LPBF process parameters can significantly influence the resulting microstructure, with layer thickness often adjusted to increase productivity and reduce manufacturing costs [1].

In [2], the effect of layer thickness on defect formation, microstructure, crystallographic texture, and mechanical properties of AlSi10Mg alloy fabricated by high-power laser powder bed fusion (HP-LPBF) was investigated. By increasing the layer thickness from 0.05 to 0.25 mm, the authors reported a substantial increase in the build rate, accompanied by changes in densification behavior, grain morphology, and texture evolution. Thicker layers promoted a transition from columnar to more equiaxed grains and a reduction in texture intensity, while the tensile properties exhibited a non-monotonic dependence on layer thickness, resulting from the combined effects of relative density and microstructural refinement.

Similar trends were observed in a previous study by the authors [3], which examined the influence of LPBF layer thickness on the microstructural evolution and mechanical behavior of AlSi7Mg aluminum alloy. In particular, increasing the layer thickness led to a transition in the morphology of Fe-rich intermetallic phases from acicular β-AlFeSi to globular π-AlFeMgSi. These microstructural changes resulted in higher strength and hardness but reduced ductility and toughness, highlighting

the key role of layer thickness in tailoring the balance between microstructure and mechanical performance in LPBF-processed aluminum alloys.

Despite advances in LPBF processing, machining remains an essential post-processing step for aluminum alloy parts, making it crucial to understand how LPBF parameters influence subsequent machining behavior. Among machining parameters, lubrication and cooling conditions have gained considerable attention due to their ability to control surface integrity, in addition to reducing friction and heat generation during cutting operations.

In [4], tool wear and surface integrity during milling of LPBF-produced AlSi10Mg alloy were investigated under dry, flood, minimum quantity lubrication (MQL), and cryogenic cooling conditions. In terms of surface roughness (Ra), CO_2 cryogenic cooling outperformed dry and flood lubrication but resulted in higher Ra values than MQL. The improvement was primarily attributed to the reduction in cutting temperature; however, the associated temperature drop also promoted surface defect formation. The reduced performance of CO_2 cooling was linked to increased workpiece brittleness at low temperatures, which facilitated chip fragmentation but adversely affected surface quality. Regarding subsurface microstructure, cryogenic machining produced more densely packed grains than the other cooling conditions, an effect attributed to rapid thermal cycling induced by the chilled gas, although limited mechanistic interpretation was provided.

High-speed machining tests conducted on AA7075-T6 aluminum alloy under dry and cryogenic conditions in [5] showed improved surface roughness under dry machining compared to cryogenic cooling. In addition, significant grain refinement was observed near the machined surface, defining an affected layer whose thickness decreased with depth from the machined surface. Under dry machining, this layer ranged from 97 to 142 μm and increased slightly with the feed rate, whereas cryogenic machining consistently resulted in a thinner affected layer. These findings were attributed to the reduced ductility of the alloy at low temperatures; under cryogenic cooling, the material exhibited a more brittle response, limiting its capacity for plastic deformation before fracture.

Overall, the literature indicates that the benefits of cryogenic cooling in machining aluminum alloys remain inconclusive. This uncertainty is even more pronounced for additively manufactured aluminum alloys, where, to the best of the authors' knowledge, only limited studies have been reported. In [3], improved machinability, evidenced by lower cutting forces, reduced force variability, smoother surface finish, and a thinner subsurface plastically deformed layer, was observed when machining LPBF AlSi7Mg samples produced with higher layer thickness. Similar results were found in [6]. In [7], the effect of hatch spacing in LPBF on the microstructure and machining response of AlSi7Mg aluminum alloy was investigated. Increasing hatch spacing promotes coarser grains, modifies melt pool geometry, and alters silicon precipitation behavior after heat treatment. While average cutting forces remain largely unaffected, larger hatch spacings reduce force variability and significantly improve surface finish.

Within this context, the present study investigates the effect of cryogenic machining on the surface integrity of LPBF-produced AlSi7Mg samples fabricated with different layer thicknesses. Cylindrical specimens were manufactured via LPBF and subsequently machined under fixed cutting conditions using either conventional flood cooling or cryogenic cooling. Surface integrity was evaluated in terms of surface roughness, surface defect morphology, and machining-induced microstructural alterations, while cutting forces were simultaneously recorded.

Materials and Methods

LPBF and heat treatment of AlSi7Mg samples. Specimens were fabricated using AlSi7Mg powder on a SISMA MYSINT100™ LPBF machine. The feedstock powder had a particle size distribution ranging from 20 μm to 63 μm, with a median particle size (D50) of 40.5 μm. Although the median particle size is slightly larger than the selected layer thicknesses, adequate powder spreading was achieved due to the broad particle size distribution [8]. Energy-dispersive X-ray spectroscopy (EDS) was employed to characterize the elemental composition of the powder, with the resulting chemical analysis reported in Table 1.

The LPBF system was equipped with a Ytterbium fiber laser with a 30 μm spot diameter and operated within a chamber filled with ultra-high-purity argon (>99.99%).

Different specimen geometries, namely cubic, tensile, and cylindrical, were fabricated according to the specific objectives of the work.

Cubic specimens with a volume of 1 cm^3 were produced for microstructural characterization.

Four round tensile specimens, designed in accordance with ASTM E8/E8M–25 standards, were fabricated to evaluate tensile properties, with their principal axis aligned parallel to the building direction.

Finally, three cylindrical specimens, each 20 mm in diameter and 70 mm in length, were manufactured for each LPBF parameter set for machining trials, with their axes oriented parallel to the building direction to ensure representative process-orientation effects.

The processing window for LPBF of AlSi7Mg was identified in a previous study [7] based on the criterion of maximum densification. After determining the optimal set of process parameters, the layer thickness was varied within a range close to this optimal condition, while remaining within the limits specified by the machine manufacturer. In particular, the layer thickness was varied between 20 and 30 μm. The decision to vary the layer thickness was motivated by the fact that, among the process parameters investigated for Al–Si alloys, layer thickness has been less extensively studied in the literature compared to laser power and scanning speed.

The LPBF process parameters are reported in Table 2. It is worth noting that, hereafter, samples processed with a layer thickness of 20 μm will be referred to as L20, those with a layer thickness of 25 μm as L25, and those with a layer thickness of 30 μm as L30.

Fabrication was performed using the chessboard scanning pattern, which was chosen and set at 3 mm x 3 mm, with layers rotated 67° from each other, according to [9].

All the samples were detached from the baseplate by using a high-precision micro-cutting machine Metkon Micracut 200 S.

After LPBF, the samples underwent a T6 heat treatment, consisting of solubilization at 535 °C for 3 hours followed by artificial aging at 150 °C for 6 hours in an argon atmosphere, to mitigate residual stresses induced by LPBF and promote precipitation hardening for enhanced material strength.

Table 1. Chemical composition of the AlSi7Mg powder (wt%).

Al	Si	Mg	Fe	Cu	Zn	Ti	Mn
Bal	6.86	0.58	0.14	0.01	0.03	0.14	0.0004

Table 2. LPBF parameters.

Laser power (W)	170
Scanning speed (mm/s)	1056
Hatch spacing (μm)	175
Layer thickness (μm)	20/25/30

Mechanical characterization of the LPBF AlSi7Mg samples. A hydraulic MTS™ 322 dynamometer was used to carry out tensile tests at a constant strain rate of 1.2 min^{-1} at room temperature. The tensile axis of each specimen was along the sample length, which was parallel to the building direction.

Machining of the LPBF AlSi7Mg samples. The heat-treated cylinders were longitudinally turned on a Mori Seiki NL1500™ lathe using PVD-TiAlN coated VCEX 11 03 01L-F 1125 turning tools, provided by Sandvik Coromant™. A fresh tool was used for every machining trial to prevent tool wear effects. A 9129AA Kistler™ three-component piezoelectric dynamometer was used to acquire the cutting forces (cutting force/Fc, radial force/Fr, and thrust force/Ft) at a sampling rate of 2500 Hz. During acquisition, a low-pass filter was used with cutoff frequencies of 300 Hz for Fc and Fr, and 600 Hz for Ft, as suggested by the dynamometer's producer guidelines. After acquisition, the force

signals were filtered with a 2nd-order low-pass filter with a cutoff frequency set at 25 Hz to remove undesired noise.

A preliminary roughing step, involving the removal of a 0.5 mm depth of cut, was carried out before the finishing pass to reach the target depth. Afterwards, the finishing step was performed using the following cutting parameters: cutting speed Vc = 200 m/min, feed f = 0.03 mm/rev, depth of cut d = 0.25 mm, longitudinal cutting length Lc = 6 mm, which were selected in accordance with the tool manufacturer's guidelines. Conventional flood lubrication was employed using a water-based fluid with 5% semi-synthetic oil (Astro-Cut HD XBP, Monroe Fluid Technology), supplied to the cutting zone by spraying at 8 bar and a flow rate of 2.5 L/min. Cryogenic turning, on the other hand, involved liquid nitrogen (LN_2) as a coolant, sprayed towards the flank and rake faces of the tool via two 0.9 mm diameter copper nozzles. LN_2 was stored at a constant pressure of 15 bar inside a dewar and conveyed to the nozzles through a vacuum-insulated tube. More details about the cryogenic cooling apparatus can be found in [10].

Microstructure and mechanical characterization of the machined LPBF AlSi7Mg samples. The surface topographies of the machined samples were acquired using a Sensofar Metrology™ S-Neox 3D optical profiler. Subsequently, surface roughness parameters were calculated using the SensoVIEW™ software in accordance with ISO 25178 [11]. The analysis included a form-removal procedure to eliminate the cylindrical geometry induced by turning, followed by band-pass filtering with an S-filter of 2.5 μm, an L-filter of 0.8 mm, and a sampling length of at least 4 mm. Three surface measurements were performed for each machined sample.

Three surface roughness parameters were considered: the arithmetic mean height (Sa), the reduced valley depth (Svk), and the reduced peak height (Spk). Sa represents the conventional surface roughness parameter; Svk quantifies the average depth of the valley regions, indicating the volume available for lubricant retention or debris trapping; Spk corresponds to the average height of the protruding peaks above the core surface level and is associated with the initial wear behavior of the surface.

The quality of the machined surfaces was further examined using a FEI Quanta™ 450 scanning electron microscope (SEM) to identify the presence of surface defects.

Finally, cross-sections of the machined samples were ground, polished, and etched using Weck's reagent to evaluate machining-induced microstructural alterations. High-magnification SEM images were acquired in the near-surface region to characterize the subsurface microstructure.

Additionally, electron backscatter diffraction (EBSD) analyses were performed on the machined samples using an Oxford Instruments™ CMOS-Symmetry detector integrated into a Tescan SOLARIS™ dual-beam field-emission scanning electron microscope (FE-SEM).

Results and Discussion

Mechanical properties of the LPBF AlSi7Mg samples. The true stress–strain curves reported in Fig. 1 for the samples fabricated with different layer thicknesses clearly demonstrate the influence of this printing parameter on the resulting mechanical performance. Increasing the layer thickness leads to higher mechanical strength, while the overall ductility, expressed in terms of both elongation and toughness, tends to decrease. The samples printed with the largest layer thickness exhibit an increase in ultimate tensile strength (UTS) of 40% compared to those manufactured with the smallest layer thickness. Conversely, the elongation at fracture decreases by 39% when comparing L30 to L20.

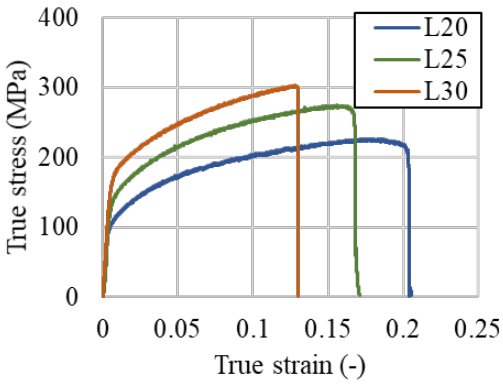

Layer thickness (µm)	UTS (MPa)	Elongation at fracture (%)	Toughness (J/mm³)
20	183 ± 6	23 ± 2	41 ± 1
25	228 ± 27	18 ± 1	38 ± 3
30	256 ± 10	14 ± 1	36 ± 3

Fig. 1. Mechanical properties of the LPBF AlSi7Mg samples at varying layer thicknesses.

Surface integrity of the machined LPBF AlSi7Mg samples. The cutting force data reported in Fig. 2a reveal distinct differences between flood and cryogenic machining conditions.

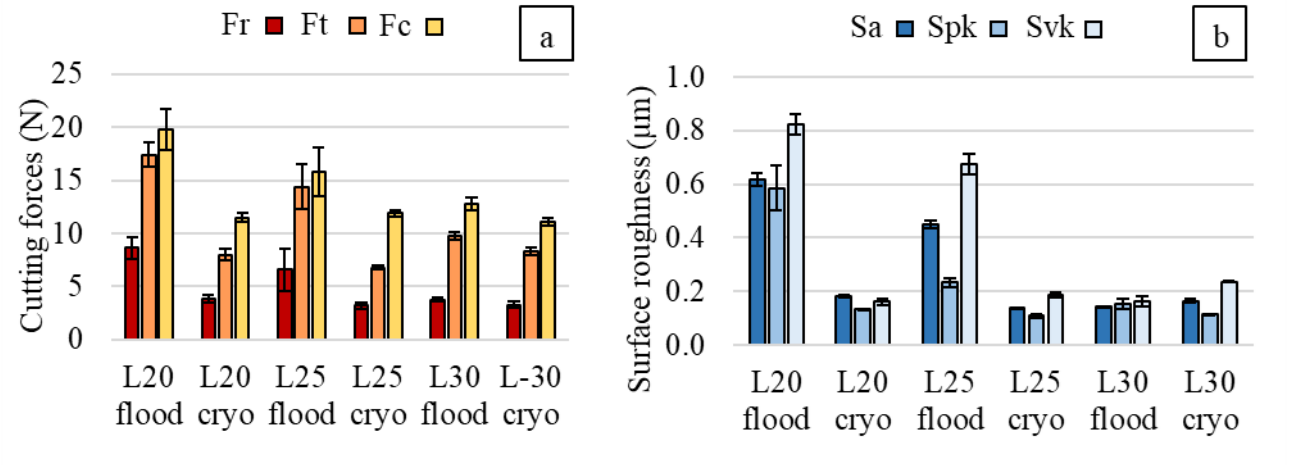

Fig. 2. a) Cutting forces and b) surface roughness of the machined AlSi7Mg samples at varying layer thicknesses and cooling conditions.

Under cryogenic cooling, all three force components are consistently lower than those measured under flood lubrication. On average, reductions of 50%, 43%, and 14% were observed for the L20, L25, and L30 samples, respectively.

This trend appears to contradict what is typically expected when liquid nitrogen is applied, as cryogenic cooling generally reduces the cutting temperature and may enhance strain hardening in the material, often resulting in increased cutting forces. A possible explanation lies in the high thermal conductivity of aluminum alloys, which promotes rapid heat dissipation from the cutting zone and reduces the effectiveness of temperature reduction under cryogenic cooling compared with other metals, where thermal effects play a more dominant role. Instead, the dominant effect of cryogenic cooling in the present case is the mitigation of tool–chip adhesion and the suppression of built-up edge formation, which are particularly critical in machining aluminum alloys [12].

With respect to the influence of layer thickness, lower cutting forces are generally associated with samples produced with higher layer thickness under flood cooling conditions. Specifically, under flood lubrication, a reduction of approximately 30% in cutting force is observed when moving from L20 to L30 samples. This trend can be correlated with the specific cutting energy: materials exhibiting higher ductility typically require higher cutting forces [3].

By contrast, under cryogenic conditions, the cutting forces appear largely insensitive to the LPBF processing parameters of the machined samples.

In addition, the variability of the measured forces depends on layer thickness. The force scatter decreases progressively from L20 to L30, with the latter exhibiting the most stable cutting behaviour. This reduced variability at higher layer thicknesses is likely attributable to decreased microstructural

anisotropy, whereas the greater anisotropy associated with lower layer thicknesses leads to more unpredictable material behaviour during machining [3].

The corresponding surface roughness parameters reported in Fig. 2b further support the benefits of cryogenic cooling. Cryogenically machined surfaces exhibit lower Sa, particularly for lower layer thickness, as well as reduced Spk and Svk values, indicating a decrease in average roughness and a diminished presence of surface peaks and valleys, respectively.

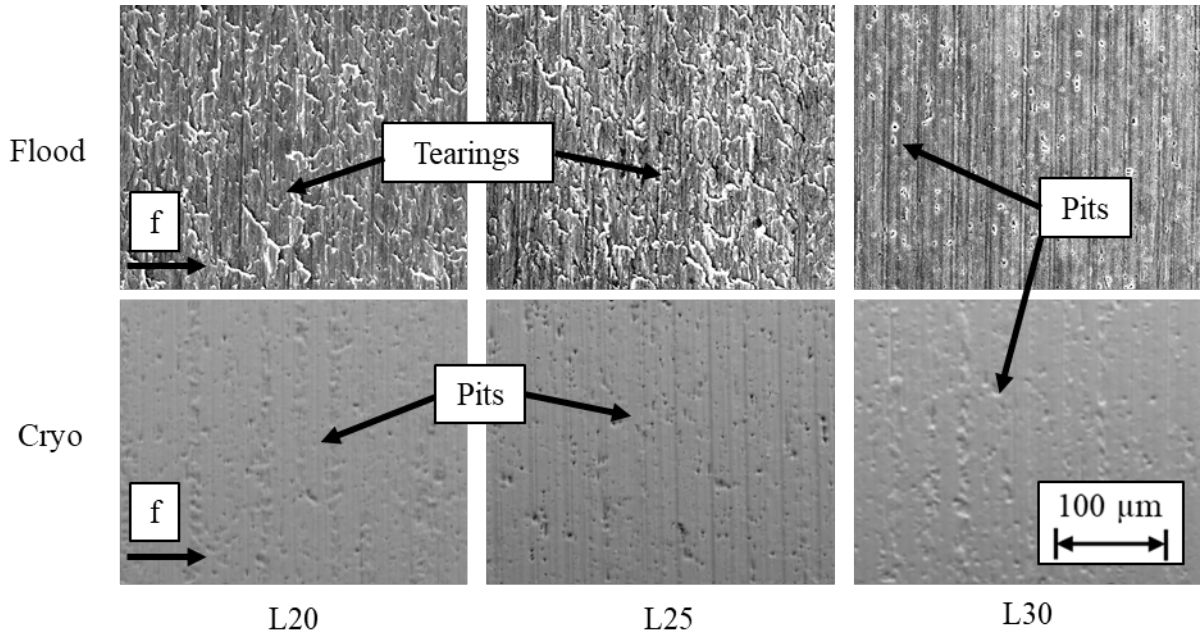

Fig. 3. SEM images of the machined surfaces of AlSi7Mg samples at varying layer thicknesses and cooling conditions.

A similar combined effect of layer thickness and cooling condition observed for the cutting forces is evident for the roughness parameters. Under flood conditions, increasing layer thickness leads to a pronounced reduction in Sa, Spk, and Svk of 77%, 74% and 80%, respectively, when moving from L20 to L30. Conversely, under cryogenic conditions, the surface roughness parameters remain nearly unchanged with varying layer thickness, showing variations of only 10% and 14% from L20 to L30 for Sa and Spk, respectively.

In general, the surface roughness results appear to be well aligned with the cutting force trends.

The SEM images in Fig. 3 provide qualitative confirmation of the defect morphology observed on the machined surfaces of AlSi7Mg samples under varying layer thicknesses and cooling conditions.

Under flood lubrication, the surfaces exhibit a higher density of tearing, particularly in samples produced with lower layer thicknesses. At the highest layer thickness, the dominant defect type shifts from tearing to pits. These pits appear as localized depressions and irregular cavities, indicative of particle undermining associated with the eutectic regions. In contrast, the surfaces machined under cryogenic cooling consistently show the same defect type, namely pits, regardless of the layer thickness.

A clear relationship between defect morphology and cutting forces emerges when comparing Fig. 1 and Fig. 3: when cutting forces exceed a certain threshold, tearing is preferentially formed, whereas lower force levels promote the formation of pits. Furthermore, the different defect types correspond to different surface roughness values, as tearing tends to increase roughness, while pits reduce it.

The metallographically-prepared cross-sections shown in Fig. 4 show the subsurface microstructural characteristics resulting from machining at different layer thicknesses and cooling strategies. In general, a thin yet clearly distinguishable plastically deformed layer (PDL) is observed immediately beneath the machined surface.

Under flood cooling conditions, the PDL is more pronounced in samples produced with lower layer thicknesses, where the deformation depth is greater and noticeable microstructural refinement

is observed. The increased deformation correlates well with the higher cutting forces and the more frequent occurrence of tearing defects discussed previously.

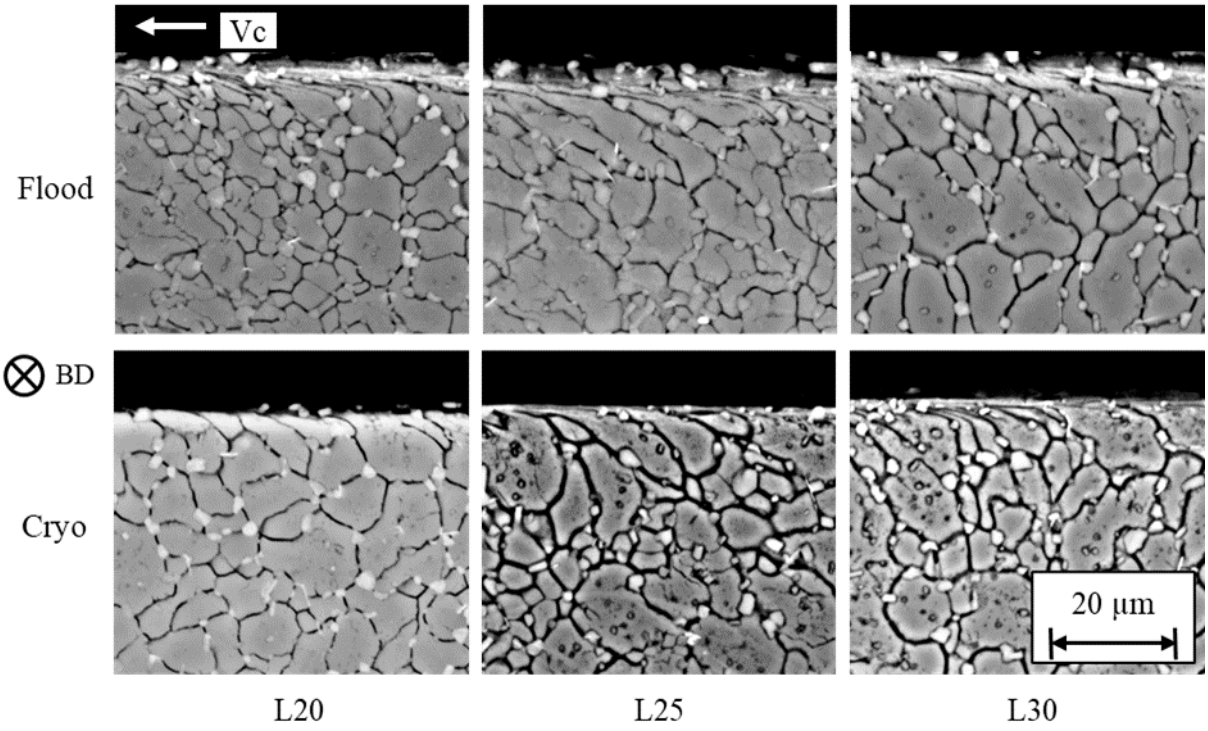

Fig. 4. Microstructure in the correspondence of the machined surfaces of AlSi7Mg samples at varying layer thicknesses and cooling conditions.

Conversely, in cryogenically machined samples, the subsurface deformation layer is slightly reduced and, in the case of L20, barely visible. This reduction in subsurface deformation is consistent with the lower cutting forces and the predominance of pit-type defects observed under cryogenic cooling.

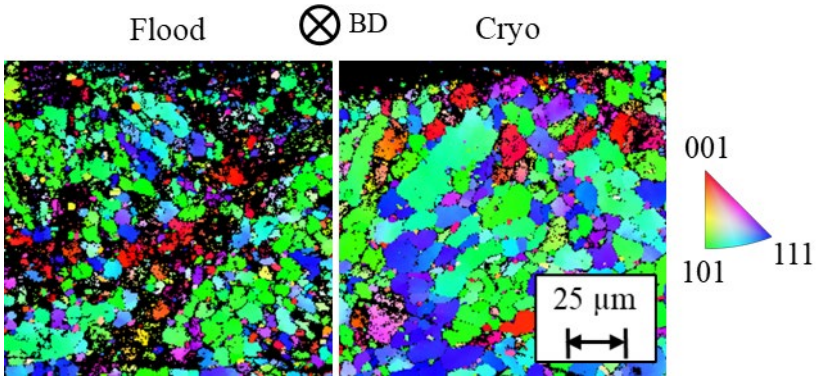

Fig. 5. EBSD analysis of the subsurface of AlSi7Mg L30 machined samples.

Fig. 5 presents the EBSD pole figures acquired in the correspondence of the subsurface of the L30 LPBF AlSi7Mg machined samples at varying cooling conditions. Both figures exhibit predominantly the same crystallographic planes, {101} and {111}, which correspond to the primary slip systems in FCC aluminum alloys.

The similarity in pole figures indicates that the deformation texture remains consistent between cryogenic and flood machining, supporting the hypothesis that cryogenic cooling did not induce a brittle deformation response despite the temperature reduction.

Summary

In this work, the influence of cryogenic machining on the surface integrity of LPBF AlSi7Mg aluminum alloy printed with different layer thicknesses was investigated.

The main conclusions can be summarized as follows:

- Cryogenic machining significantly reduced cutting forces compared to conventional flood lubrication, with the most pronounced reductions observed in samples manufactured with lower layer thicknesses.
- Surface roughness parameters (Sa, Spk, Svk) were consistently improved under cryogenic cooling, indicating enhanced surface quality and reduced surface asperities, particularly for lower layer thicknesses.
- A strong correlation was observed between cutting forces and surface integrity: higher cutting forces promoted tearing defects, whereas lower force levels favored pit-type defects, which are associated with reduced surface roughness.
- Increasing layer thickness improved machinability and surface integrity under both cooling conditions, leading to lower cutting force variability, reduced roughness, and fewer severe surface defects.
- Cryogenic machining effectively reduces machining-induced subsurface plastic deformation, resulting in a thinner affected layer and a sharper transition between the machined surface and the bulk microstructure.
- EBSD analysis revealed similar deformation textures under both cryogenic and flood machining, with dominant {101} and {111} crystallographic planes, indicating that cryogenic cooling did not induce a brittle deformation response in the FCC AlSi7Mg alloy.

Acknowledgements

The work was financed by the European Union - NextGenerationEU (National Sustainable Mobility Center CN00000023, Italian Ministry of University and Research Decree n. 1033 - 17/06/2022, Spoke 11 - Innovative Materials & Lightweighting). The opinions expressed are those of the authors only and should not be considered as representative of the European Union or the European Commission's official position. Neither the European Union nor the European Commission can be held responsible for them.

References

[1] C. Schwerz, F. Schulz, E. Natesan, L. Nyborg, Increasing productivity of laser powder bed fusion manufactured Hastelloy X through modification of process parameters, J. Manuf. Process. 78 (2022) 231–241.

[2] M. Liu, K. Wei, X. Zeng, High power laser powder bed fusion of AlSi10Mg alloy: Effect of layer thickness on defect, microstructure and mechanical property, Mater. Sci. Eng. A 842 (2022) 143107.

[3] E. Ghinatti, T. Islam, S. Pan, R. Bertolini, S. Bruschi, Effect of layer thickness on the microstructure and machinability of AlSi7Mg processed by laser powder bed fusion, CIRP J. Manuf. Sci. Technol. 64 (2026) 137–148.

[4] N.S. Ross, N. Srinivasan, M.B.J. Ananth, A.Y. AlFaify, S. Anwar, M.K. Gupta, Performance assessment of different cooling conditions in improving the machining and tribological characteristics of additively manufactured AlSi10Mg alloy, Tribol. Int. 186 (2023) 108631.

[5] S. Imbrogno, G. Rotella, S. Rinaldi, Surface and subsurface modifications of AA7075-T6 induced by dry and cryogenic high-speed machining, Int. J. Adv. Manuf. Technol. 107 (2020) 905–918.

[6] E. Ghinatti, R. Bertolini, A. Ghiotti, S. Bruschi, The role of the layer thickness on the surface integrity of LPBF AlSi7Mg after turning, Procedia CIRP 133 (2025) 90–95.

[7] E. Ghinatti, R. Bertolini, A. Ghiotti, S. Bruschi, Effect of the hatch spacing in laser powder bed fusion on the AlSi7Mg aluminum alloy cutting forces and surface finish after turning, Mater. Res. Proc. 41 (2024) 1907–1915.

[8] MA. Balbaa, A. Ghasemi, E. Fereiduni, MA, Elbestawi, SD. Jadhav, J-P. Kruth. Role of powder particle size on laser powder bed fusion processability of AlSi10mg alloy, Add. Manuf. 37 (2021) 101630.

[9] M. Wang, B. Song, Q. Wei, Y. Zhang, Y. Shi, Effects of annealing on the microstructure and mechanical properties of selective laser melted AlSi7Mg alloy, Mater. Sci. Eng. A 739 (2019) 463–472.

[10] R. Bertolini, A. Stramare, S. Bruschi, A. Ghiotti, A. Campagnolo, Impact of cryogenic machining on the fatigue strength and surface integrity of wrought Ti6Al4V with equiaxed microstructure, Eng. Fail. Anal. 170 (2025) 109274.

[11] ISO 25178-2, Geometrical product specifications (GPS) — Surface texture: Areal — Part 2: Terms, definitions and surface texture parameters, ISO, Geneva, Switzerland, 2022.

[12] F. Ahmed, F. Ahmad, ST. Kumaran, M. Danish, R Kurniawan, S Ali, Development of cryogenic assisted machining strategy to reduce the burr formation during micro-milling of ductile material, J Manuf Proc 85 (2023) 43–51.